SPACE PROPULSION 2018
BARCELO RENACIMIENTO HOTEL, SEVILLE, SPAIN / 14 – 18 MAY 2018

Novel Non-Destructive Inspection of the STAR Additively Manufactured Resistojet

C. Ogunlesi [1*], A. Grubisic [1*], F. Romei [1], M. Robinson [1], S. Ahmed [1], P. Aimone [2], F. Dary [2], D. Gibbon [3], M. Curtis Rouse [4]

(1) University of Southampton, University Road, Southampton, SO17 1BJ, United Kingdom,
(2) H.C. Starck Inc., 45 Industrial Place, Newton, MA, 02461, USA
(3) Surrey Satellite Technology Ltd., Tycho House, 20 Stephenson Road, Surrey Research Park, Guildford, Surrey, GU2 7YE, United Kingdom
(4) Satellite Applications Catapult, Harwell Campus, Oxfordshire, OX11 0QX, UK
**Emails of corresponding authors:*
C.Ogunlesi@soton.ac.uk , A.Grubišić@soton.ac.uk

KEYWORDS: resistojet, space propulsion, additive manufacturing, refractory materials, non-destructive inspection.

ABSTRACT:

The paper presents the design, manufacturing and postproduction analysis of a novel high-temperature spacecraft resistojet heat exchanger manufactured via selective laser melting to validate the manufacturing approach. The work includes the analysis of critical features of a heat exchanger with integrated converging-diverging nozzle as a single piece element. The metrology of the component is inspected using optical analysis and profilometry characterise the surface and roughness of components. A novel process of high-resolution micro-Computed Tomography (CT) is applied as a tool for volumetric non-destructive inspection and conformity checking since the complex geometry of the thruster does not allow for internal inspection. The CT volume data is utilised to produce a surface mesh on which a novel coordinate measurement technique is applied for nominal (as manufactured) to actual (as designed) inspection and analysis. A thin-wall concentric tubular heat exchanger design is determined to meet dimensional accuracy requirements through nominal/actual comparison analysis.

1. INTRODUCTION

1.1. Project Background

The aim of the research is to improve on the design and manufacturing processes of the Super-high Temperature Additive manufactured Resistojet (STAR) being developed as for an all-electric spacecraft, the benefits of which are described in [1], [2] . A resistojet is the simplest form of electric propulsion thruster, electrically heating a propellant through resistive heating of a heat exchanger for some form. In general, the higher the operating temperature of the heat exchanger, the higher the operating gas temperature and thus the specific impulse attainable by the thruster. The specific impulse of gas dynamically expanded flow is approximated below in Eq.1 assuming a fully expanded flow with negligible pressure thrust component:

$$Isp \propto \sqrt{2T_0\left(1-\left(\frac{P_e}{P_{0c}}\right)^{\frac{\gamma-1}{\gamma}}\right)} \qquad \text{(Eq. 1)}$$

Where T_0 is the stagnation temperature of the flow, P_e is the static pressure at the exit of the nozzle, P_{0c} is the stagnation pressure in the chamber prior to entry into the nozzle and γ is the ratio of specific heats. The effective exhaust velocity of propellant is given by Eq. 2:

$$V_{eq} = Isp \cdot g_0 = \frac{F}{m_{tot}} \qquad \text{(Eq. 2)}$$

Current resistojet concepts are restrained in their achievable ISP due to limitations in materials technology, as such high stagnation temperature requirements are greater than the melting point of conventional materials. The resistojet presented in this paper is a design theoretically capable of operating with propellant temperatures up to 3000K and achieving a thruster efficiency in the range of 65 – 90%. This has been made possible through utilising high melting point refractory metals in additive manufacturing processes.

From the literature, it has been concluded that the best performance for a high temperature resistojet is achieved through a recirculating flow geometry made up of concentric tubular channels [3]. However, past designs achieved this through costly and challenging manufacturing processes such as EB welding of chemical vapour deposition manufactured thin walls [4].

This paper presents a design that has been conceived and produced through additive manufacturing, specifically selective laser melting (SLM) to produce a single monolithic structure, shown in Fig. 1. This significantly reduces the complexities of manufacturing and assembling an intricate thruster, whilst enabling freedom of design. In this design, the propellant is directly heated by the walls of the thruster, which are themselves heated through resistive heating. To achieve the current-voltage characteristics needed for the heater, the walls of the heat exchanger are required to be very thin (<150µm), to give sufficient dissipation at low current.

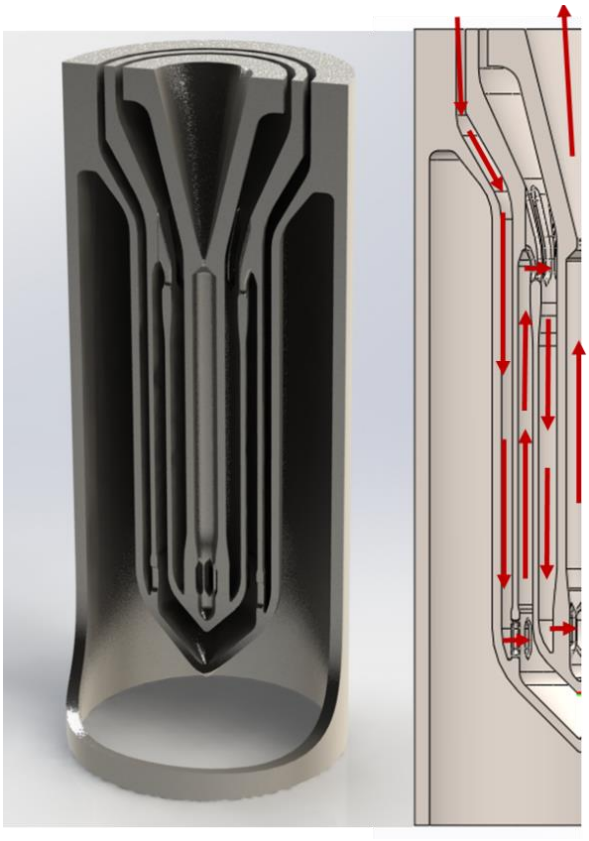

Figure 1: (left) 3D model with cutaway showing the recirculating flow geometry of the resistojet (right) Xenon flow path in the thruster

Past studies of the STAR have been focused on the design and performance of the thruster [5] [6], and thus utilised a resistojet printed in the better understood stainless steel. This paper presents the first STAR printed in a refractory metal and will focus on how well the build met the design criteria and quality requirements.

1.2. Surface Roughness

Surface roughness may be quantified as the degree to which an actual surface deviates from its ideal form [7]. The greater the deviations from this ideal form, the rougher the surface. Surface roughness represents an extremely important characteristic when evaluating the effectiveness of heat transfer of micro-fluidic channels (<1mm). As surface roughness increases, heat transfer between the fluidic channel and the fluid itself was found to increase [8], [9]. It was also shown in several instances that the heat transfer improved significantly as the flow transitioned from laminar to turbulent [8], [9]. This increase in heat transfer may be due to the increase in surface area with higher surface roughness. This thus results in a higher wetting area between the fluid and microchannels increasing the effectiveness of the heat transfer.

It was also reported that surface roughness has a large effect on the flow characteristics of fluids within microchannels [9].The friction factor, which relates to the amount of energy a fluid loses as it flows through a pipe due to frictional forces, was found to increase with surface roughness. Roughness on the surface of a channel was reported to act as an additional disturbance source to the flow, disrupting the boundary layer. This thus results in a disturbance in the main fluidic flow increasing the pressure drop across the channel. This was reported to be particularly true for high mass flow rates. The effect of surface roughness on macrochannels however was found to be insignificant for both heat transfer and pressure drop [9].

The STAR is to be printed as a single monolithic piece, with as little post processing as possible. This presents challenges when manufacturing the thruster as a compromise will need to be found between a higher surface roughness for the inner fluidic channels, and a lower surface roughness for the nozzle area. Reports from the literature indicate that a limitation of SLM is the high surface roughness of the parts printed, commonly around 20µm and usually requiring post processing [10]. As this is being designed to meet certain standards developed by Surrey Satellite Technologies Ltd, the nozzle section will need to have a finish value of at least N7 (R_a = 1.7µm, R_t = 8µm).

1.3. Selective Laser Melting

Selective Laser Melting (SLM) is a powder bed additive manufacturing process capable of producing high density, complex metal components from metallic powders whilst reducing time, cost and energy requirements associated with more traditional methods [10], [11]. A high intensity laser is used to melt and fuse together powder particles in a sequence of layers. The first layer is built on a substrate plate in an inert atmosphere within a

building chamber. A layer of powder is laid over the substrate plate and the high intensity laser melts and fuses selected areas of this powder according to 3D model data. Once this layer has been completed, the substrate plate is lowered and a new layer of powder deposited on top [10]. After the laser then melts the next layer of powder, this process is repeated until the metal component is entirely built. SLM allows for the fabrication of small components with high resolution features (layer thickness of 20µm - 100µm [10], [11] and was deemed most suitable for this project as opposed to other additive manufacturing techniques [3] [12].

Despite the advantages of SLM over traditional manufacturing methods, there remain challenges when constructing a component through additive manufacturing. Laser power, scanning speed, hatch spacing and layer thickness are parameters that can be manually adjusted to optimise the quality of the print and are directly related to the amount of energy available to heat up the powder [10]. Balling, molten metal forming into spheres due to surface tension and poor wetting of the layer, is a common defect of SLM resulting in rough, porous surfaces. Large amounts of residual stresses can also be built up in components manufactured through SLM due to the large thermal gradients they endure. This may lead to crack formation or delamination of layers in order to relieve the stress. This is a particular problem for overhanging or protruding features as they are not to directly connected to the build plate during printing, making them less resistant to thermal shock [11]. Refractory metals are ideal materials to build the STAR as they are electrically conductive and can operate at temperatures in excess of 3000K [3]. Despite the high melting temperature and low wettability of refractory metals, past studies have proven them capable of producing fully dense components through SLM [3], [10].

Table 1: Overview of mechanical properties of pure Ta [13], [14]

Ta grade	Commercial pure Ta EB[(a)]	Commercial pure, P/M[(b)]
Modulus of elasticity (GPa)	185	185
Vickers hardness (Hv)	110	120
Ultimate tensile strength (MPa)	205	310
Yield strength (MPa)	165	220
Elongation (%)	40	30

(a) EB, electron beam furnace melted
(b) (b) P/M, powder metallurgy

Tantalum is a very hard and ductile refractory metal with a high melting point (2996°C) and density (16.69gcm^{-3}) [13]. An overview of its mechanical properties is shown below in Tab. 1. The unique solidification conditions caused by SLM result in large columnar grains across the layers of the component resulting in a large yield strength anisotropy. These qualities as well as the numerous studies already conducted on the behaviour of tantalum SLM produced components [13], [14] make tantalum an ideal material to manufacture the first refractory resistojet.

1.4. X-ray CT Scanning

In CT scanning, the term artefact is used to refer to any discrepancy between the actual points of the scanned object, and the reconstructed points of the CT image [15]. As the software used to reconstruct the image from the radiographs cannot differentiate between actual and erroneous data, any error in the measurement will reflect itself as an error in the reconstructed image.

Beam hardening is a common artefact of CT scanning, and occurs as low energy X-ray photons are more easily attenuated than high energy photons, thus the mean energy of the beam increases as it passes through the object [15]. This is particularly a problem with high atomic number materials, such as refractory metals. This results in more X-ray beams reaching the detector than intended, causing dark streaks in the resulting radiographs along the direction of greatest attenuation. Artefacts from beam hardening can manifest themselves in different ways, depending on the location, spacing and depth of the high attenuation objects. They can appear as dark and light streaks between two high attenuation objects, or as dark streaks along the long axis of single high attenuation objects. For low energy X-rays, attenuation is primarily due to the photoelectric effect, and is proportional to Z3/E3, where Z is the atomic number and E is the energy. At higher energies, attenuation is due to Compton scattering and is proportional to 1/E. Compton scattering causes X-rays to change direction, scattering to a different detector than intended.

1.5. Research Objectives

The current design for the STAR was previously developed by Federico Romei [3] [16] [17] and utilises a recirculating flow geometry and incorporates an integrated nozzle. The thickness of the walls of the heat exchanger are on the order of 100µm in order to achieve the current – voltage characteristics necessary for the design. The thinner the walls the greater the resistive dissipation. Previous versions of the STAR were printed in 316L stainless steel as it shares similar resistivity to refractory metals. The STAR has undergone previous manufacturing verification exercises in order to optimise the design for printing in 316L stainless steel [18] and is currently undergoing endurance testing [19]. This same design was used to print the tantalum resistojets for this investigation.

As this thruster is the first of its kind to be printed through SLM in tantalum, it requires manufacturing verification to ensure that the complex design has been maintained and to explore the limitations of the technology. Previous studies have shown that it is indeed possible to produce high density components of at least 100µm thickness in refractory metals, as required for this thruster [1], [8]. The focus of this investigation was thus to utilise non – destructive analytical techniques to evaluate the surface and overall quality of the tantalum build. Both a full build and a sectioned version of the thruster underwent analysis in this investigation. The purpose of printing these two designs was so that surface characterisation techniques could be carried out on the inner channels of the heat exchanger without having to section the heat exchanger, which might affect the surface finish of the print.

2. ROUGHNESS CHARACTERISATION

2.1. Test methodology

Optical interferometry was performed using an Alicona InfiniteFocus to collect topographical information about the resistojet. Measurements were taken at six different locations on the sectioned part, the locations of which are shown below in Fig. 2. To build up accurate datasets about the most critical locations on the part, three images were captured in the nozzle area and three within the inner heat exchanger tube. Similar measurements have been performed on past versions of the STAR. Each of the below images were captured using 10X magnification.

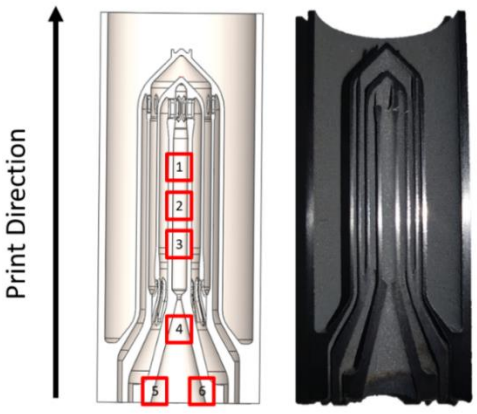

Figure 2. Tantalum resistojet CAD model (left) and photo (right) detailing the measured areas for surface roughness characterisation.

As well as the tantalum build, surface characterisation was also performed on a steel thruster of the same design, as the surface characteristics of the steel thruster are already well understood and thus suitable for comparison against the tantalum thruster.

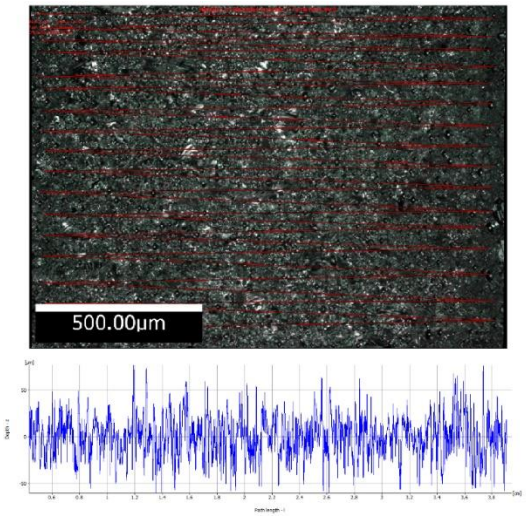

Figure 3. Example of the profile roughness measurement taken with the Alicona from location 1. (Top) Evaluation path of the profile roughness measurement (bottom) vertical position of the surface versus the path length

After capturing the 3D image data, form removal techniques were applied to the data to obtain the average surface roughness. For the images taken in locations 1, 2 and 3, the form removed was cylindrical, whilst for locations 4, 5 and 6, the form removed was conical. The software supplied with the Alicona automatically calculated the form that best fit the chosen area and applied the appropriate form removal technique as seen in Figure 4. Analytical techniques were then applied to the resultant form removed datasets in order to obtain the surface profile roughness (R_a) and surface area roughness (S_a) values. The exact values of these parameters, as well as the respective root mean square profile and area roughness (R_q and S_q respectively) are shown below in Tab 2 and Tab.3,

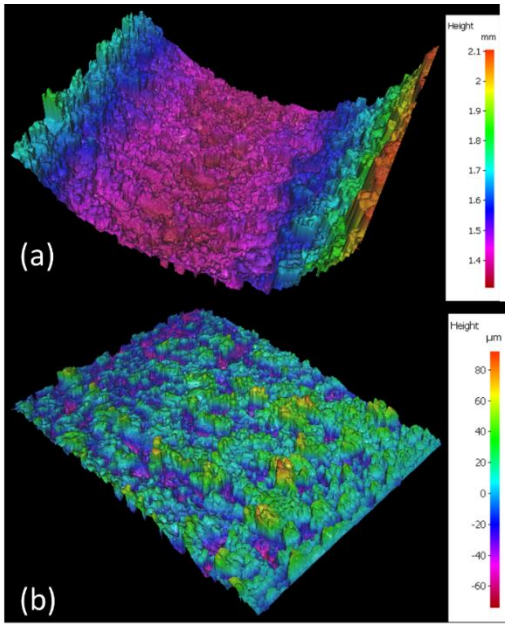

Figure 4. 3D surface scans of location 1 (a) without form removed (b) with form removed (Alicona InfiniteFocus,10x objective)

which show the profile roughness measurement values for both the steel and tantalum resistojets, calculated from the form removed datasets. To comply with ISO standards to generate a roughness profile, it was necessary to suppress long wavelengths from the primary profile using a high pass Gaussian profile filter with a cut off wavelength equal to L_c which is itself equal to the evaluation length [20], [21]. Doing so made the resultant profiles comparable to measurements made using tactile instruments.

After establishing an evaluation length on a sample area, an example of which is shown in Figure 3, the software automatically calculated which ISO standards the measurement conformed to.

2.2. Results

The Alicona InfiniteFocus is an optical interferometer that was used to measure the surface roughness of the heat exchanger and acquire 3D topographical information about the surface. The Alicona operates through combining the small depth of focus of an optical microscope with vertical scanning. This allows it to provide topographical and colour information due to variation in the focal length [22].

Although this technique does enable vertical resolution of up to 10nm [23], it is limited due to the fact that the images are captured from directly above the examined surface, meaning that it is unable to capture shadowed or angled areas. This error is clearly visible in the below image, Figure 5. This thus may have resulted in an error when calculating surface area. The settings used to capture these images were 1µm for the vertical resolution and 3µm for the lateral resolution.

The value R_a may be defined as the arithmetic mean value of the deviation of the actual form from the idea centre line and is calculated through Eq. 3 where L is the path length and N the number of samples.

$$R_a = 1/L \sum_{n=1}^{N} |r_n| \qquad \text{(Eq. 3)}$$

It can be seen from the above data in Tab. 2 that for each of the corresponding locations on both the tantalum and steel resistojets, this deviation is notably larger for the tantalum resistojet. For both datasets the spread of the results is small, each set of roughness values corresponding to an ISO roughness value of N10 (R_a = 12.5µm, R_t = 50µm).

Table 2. Profile roughness measurements of the 3D form removed data for the steel and tantalum resistojets

Area	Lc (µm)		ISO		Ra (µm)		Rq (µm)	
	Steel	Tantalum	Steel	Tantalum	Steel	Tantalum	Steel	Tantalum
1	8000	8000	4287/4288	4287/4288	15.23	16.87	19.5	21.32
2	8000	8000	4287/4288	4287/4288	13.27	15.93	17.15	19.93
3	8000	2500	4287/4288	4287	13.59	17.47	17.8	22.98
4	8000	2500	4287/4288	4287	15.59	16.45	19.58	21.87
5	8000	8000	4287/4288	4287/4288	13.01	16.97	16.81	22.05
6	8000	8000	4287/4288	4287/4288	13.67	24.48	17.01	35.46

Table 3. Surface texture measurements of the 3D form removed data for the steel and tantalum resistojets

Area	Area ratio		Projected area (mm)		Sa (µm)		Sq (µm)	
	Steel	Tantalum	Steel	Tantalum	Steel	Tantalum	Steel	Tantalum
1	2.00	2.05	1.55	1.54	15.11	16.91	19.52	21.36
2	1.93	2.00	1.44	1.55	13.59	16.77	17.89	21.07
3	1.94	2.11	1.52	1.51	13.37	18.50	17.51	24.55
4	1.93	2.07	1.55	1.55	16.67	18.72	21.35	25.71
5	1.85	2.24	1.55	1.53	13.66	21.82	17.53	33.28
6	1.90	2.29	1.55	1.53	15.62	49.7	19.53	71.33

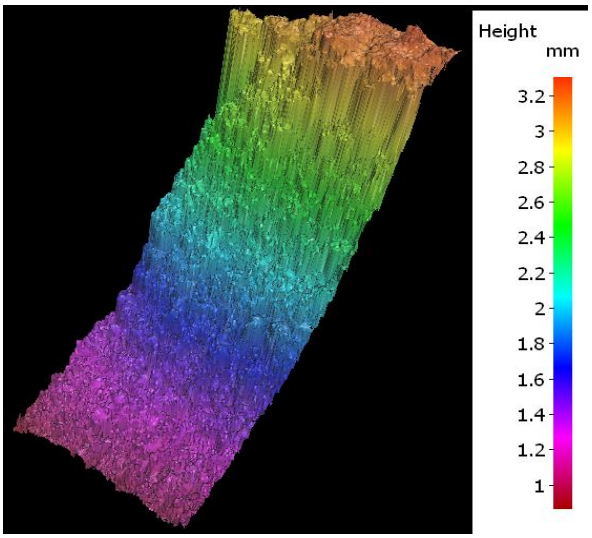

Figure 5. 3D surface scan of nozzle section showing the measurement error at loc. 6 (Alicona InfiniteFocus, 10x)

The data shows significant homogeneity of the results with no notable trends. The spread of the values for the tantalum resistojet is slightly larger, with a notable value in location 6 within the nozzle of the resistojet. The increased roughness in in tantalum at point 6 is not shared by steel samples. S_a is the deviation of each point on the surface from the arithmetic mean of the surface [24], and is calculated through Eq. 4

$$S_a = 1/A \iint_A |Z(x,y)| dxdy \qquad \text{(Eq. 4)}$$

In Tab. 3 is the ratio between the measured surface area and the corresponding ideal forms (cylindrical for locations 1-3, conical for locations 4-6). As the roughness of the actual surface increases, so does its surface area. This thus leads to an increase in area ratio. Locations 5 and 6 show the largest area ratios, the actual surface area of location 6 being 229% larger than the ideal surface area.

Whilst locations 5 and 6 show the highest area ratios on the tantalum thruster, these same locations show the lowest area ratios on the steel thruster. For both the inner channel and nozzle locations, a higher area ratio corresponds to a higher average surface area roughness. A higher S_a value is also seen to correspond to a higher RMS surface area value, S_q.

3. NON-DESTRUCTIVE INSPECTION USING CT SCANNING

3.1. Hutch CT Scanning System

X-ray CT scanning was performed in the µ-VIS X-Ray Imaging Centre which also provided the necessary software packages to analyse the images. Radiographs were taken using a custom 450/225 kVp Hutch CT system, shown in Figure 6. This scanner is equipped with two micro-focus X-Ray sources (450kVp and 225kVp) and two X-ray detectors; a 2000x2000 pixel flat panel detector and a 2048 pixel Curved Linear Detector Array (CLDA). The dimensions of the scanned specimen can range from a few millimetres in cross section up to 1 x 1 x 1.5m, and up to 100kg in mass. The 225kVp source has a series of anodes that allow for different combinations of spot size and flux characteristics. The main properties of used to scan the resistojet are shown below in Tab. 4.

Table 4. Main properties of the CT scans performed on the tantalum resistojet

Parameter	Value
Image dimension	2000 x 2000 x 2000 = 8000000000 voxels
Resolution of x, y and z axis	0.025338206mm
Angular step	0.149937526°
Number of projections	2401

The spatial resolution achieved for this scan was approximately 25.3µm, with 2401 radiographs taken by rotating the collimator around its central axis with an angular step of approximately 0.15°.

VG Studio MAX was used for initial visual inspection of the resulting radiographs and to reconstruct these into a full 3D image, as seen in Figure 7. A surface extraction tool in the software was then used to export a mesh of this 3D surface into the software GOM Inspect V8, which was then used to perform nominal to actual comparison against a CAD model of the thruster.

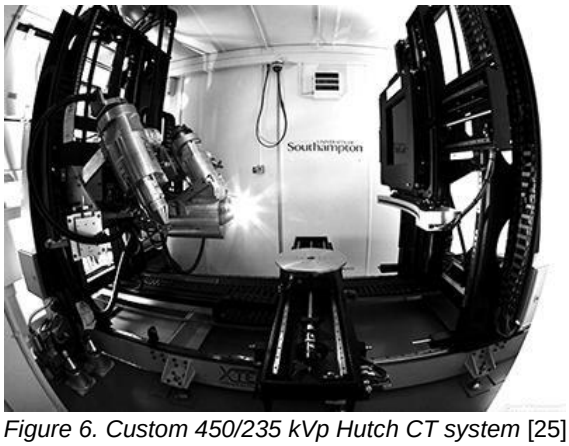

Figure 6. Custom 450/235 kVp Hutch CT system [25]

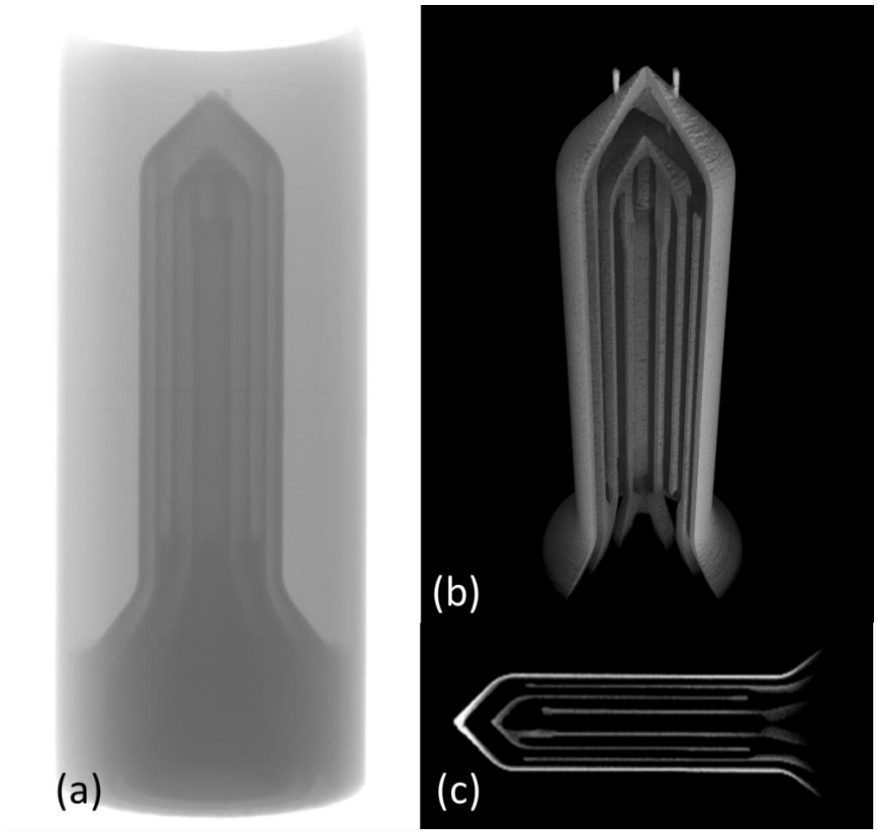

Figure 7: (a) X-ray radiograph of the tantalum resistojet where higher density areas appear darker (b) 3D reconstruction of the resistojet (c) 2D radiograph slice

Due to the difficulty of CT scanning refractory metal components, the nozzle and outer casing of the thruster were unable to be accurately imaged, as seen in Fig. 7 because of beam hardening effects. Due to the poor quality of these sections, they have been omitted from the reconstructed radiographs that will be analysed in this paper.

3.2. Actual to nominal comparison

After importing the surface mesh of the thruster into GOM Inspect V8, the surface was aligned to the CAD model. Best fit cylinders were overlaid onto the inner channels of the actual surface using a Gaussian best-fit method and were then compared against the nominal values. The resulting values can be seen below in Tab. 5, the corresponding tubes shown in Fig. 8.

The maximum deviation can be seen at cylinder 1's internal surface, reaching a maximum of 90µm. Although this is still an acceptable deviation, this is an anomalous result as the majority of the other surfaces show good agreement with the CAD geometry and deviations less than 80µm.

A trend can be seen that the thickness of the actual walls is less than thickness of the walls of the CAD model. This indicates that the walls of the STAR have shrunk after printing. An exception to this trend are the innermost walls of the heat exchanger, cylinder 1. The walls of cylinder 1 show the greatest deviation as they are 80µm thicker than the nominal. Despite these trends, the thicknesses of all of the heat exchanger walls are within acceptable bounds for the purposes of the STAR.

Table 5: Deviation of the heat exchanger channel radii from nominal radii of the CAD model

Cylinder	Nominal (mm)	Actual (mm)	Deviation (mm)	Thickness deviation (mm)
1 in	1.62	1.53	-0.09	-0.08
1 out	2.33	2.32	-0.01	
2 in	4.12	4.13	0.01	0.03
2 out	4.67	4.65	-0.01	
3 in	6.02	6.03	0.01	0.02
3 out	6.6	6.59	-0.01	
4 in	7.5	7.51	<0.01	0.04
4 out	8.47	8.44	-0.03	

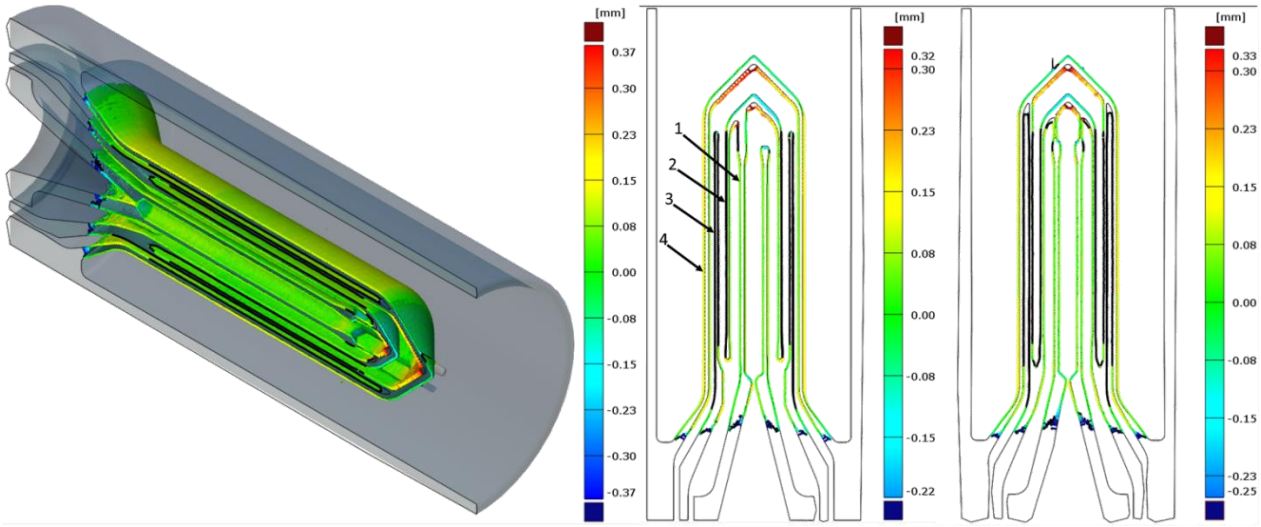

Figure 8: (Left) CAD model overlaid on actual surface and (right) Axial sections of the thruster orthagonal to each other

Fig. 8 shows the overall deviation of the actual surface with the CAD model overlaid. From this it can be clearly seen that the majority of the surfaces, including the micro-fluidic channels that make up the bulk of the thruster are very accurate to the original CAD design with deviation of these channels within the mid-section of the thruster varying only between 80µm - 90µm.

Greater deviation can be seen at the top end of the thruster where the heat exchanger converges towards a point.

For ease of inspection, the thruster has been separated into different stages for analysis, each of which are highlighted below in Fig. 9.

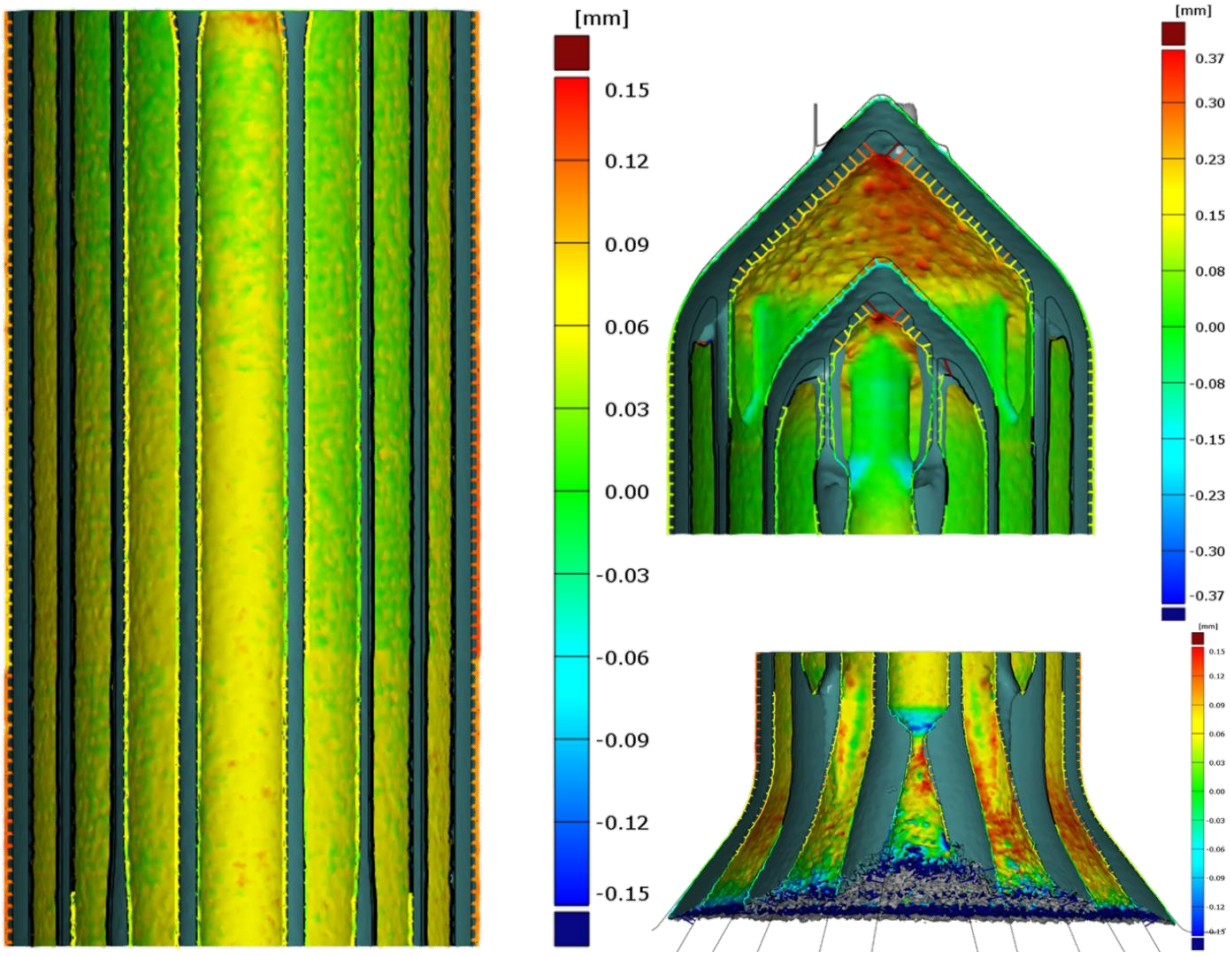

Figure 9: Actual surfaces of the heat exchanger with colour maps denoting deviation from nominal surface

The surface and walls of the microfluidic channels of the heat exchanger as seen in Fig. 9 show little deviation from the CAD design, with the majority of the actual surface deviating less than 90µm from the nominal surface. Greater deviation is seen on the walls of the outermost channels which deviates up to approximately 130µm outwards from the nominal surface.

The nozzle and inflow regions as shown in Figure 9 show good corroboration with the nominal surface, with the fluidic channels showing deviations between 60 µm – 90 µm. The greatest deviations in this region occur as the channels diverge outwards to form the nozzle. At these bends the surface begins to show notably greater deviation of up to 150 µm and irregularity in the surface quality. This is of particular interest as this is a critical region for fluid flow. As previously stated, due to beam hardening effects it was difficult to obtain accurate radiographs of the nozzle and inflow region. As a result much information about the surface in the nozzle region was lost and the accuracy of the resulting measurements is uncertain.

Similarly to the inflow regions, the greatest deviations from the CAD are on the end of the heat exchanger in both the inner and outer fluidic channels where the thruster curves towards a point, as seen in Figure 9. Here there is significant shrinkage of the actual surface up to 370µm. This is most likely due to the fact that these are overhanging regions, with only the metallic powder underneath them as support as these regions were being printed. This may have resulted in a large amount of residual stress build up resulting in irregular features and shrinkage on the underside of the printed surface, as seen in the above figures. However unlike the inflow region, the deviations in this region are acceptable for this project as the fluid flow in these regions is not critical.

4. CONCLUSIONS AND FUTURE WORK

The tantalum thruster presented in this research was a first attempt at manufacturing the STAR in a refractory metal. The manufacturing and non – destructive evaluations have provided valuable information on the capabilities and limitations of SLM of refractory metals.

The surface roughness of the tantalum resistojet was notably higher than that of the stainless steel resistojet in all measured areas. Profile roughness measurements showed no notable trends in the roughness measurements for the different areas of the thruster. The surface area measurements however showed a slight increase in average surface roughness at the nozzle and inflow regions. This was to be expected due to the high build angle of this region.

X-ray CT scanning of the component proved successful, providing clear images of the microfluidic channels within the thruster. However higher density material regions such as the nozzle an outer casing proved difficult to image clearly and were thus removed from the radiographs when analysing the results. Actual to nominal comparison showed that the majority of the thruster was very accurate to the original CAD model, deviating less than 150µm. The regions that showed the greatest deviation were the inflow and heat exchanger tip, which deviated up to 370µm from the nominal. This was most likely due to the steep build angle of these regions.

Overall this novel investigation of a tantalum component has proven promising for the future development of the STAR in SLM produced refractory metals. Further investigation will need to be carried out on the surface qualities of the inflow region of the thruster.

5. ACKNOWLEDGEMENTS

This work was carried out as part of a PhD program funded through the EPSRC (Engineering and Physical Sciences Research Council). Additional funding was provided by the National Space Technology Programme 2 from the UK Space Agency, as part of the RADICAL (Refractory Additive Layer Manufacturing for Commercial Space Applications) project. The authors are grateful for the assistance of Dr. Mark Mavrogordato from the University of Southampton µ-VIS X-Ray Imaging Centre with non – destructive inspection.

6. REFERENCES

[1] M. Coletti, A. Grubisic, C. Collingwood, and S. Gabriel, “Electric propulsion subsystem architecture for an all-electric spacecraft,” in *Advances in Spacecraft Technologies*, InTech, 2011.

[2] A. N. Grubisic and S. B. Gabriel, “Assessment of the T5 and T6 hollow cathodes as reaction control thrusters,” *J. Propuls. Power*, no. null, pp. 810–820, 2016.

[3] F. Romei, A. N. Grubišić, and D. Gibbon, “Manufacturing of a high-temperature resistojet heat exchanger by selective laser melting,” *Acta Astronaut.*, vol. 138, no. April, pp. 356–368, 2017.

[4] P. J. Sherwood, “Construction of a High Performance Resistojet for Satellite Propulsion.” 1978.

[5] F. Romei, “Multiphysics model validation of resistojets with concentric tubular heat exchanger,” pp. 1–15, 2017.

[6] F. Romei, A. Grubisic, D. Gibbon, O. Lane, R. A. Hertford, and G. Roberts, “A Thermo-Fluidic Model for a Low Power Xenon Resistojet,” 2015.

[7] “Roughness measurements of stainless

steel surfaces."

[8] X. Yuan, Z. Tao, H. Li, and Y. Tian, "Experimental investigation of surface roughness effects on flow behavior and heat transfer characteristics for circular microchannels," *Chinese J. Aeronaut.*, vol. 29, no. 6, pp. 1575–1581, 2016.

[9] S. G. Kandlikar, S. Joshi, and S. Tian, "Effect of surface roughness on heat transfer and fluid flow characteristics at low Reynolds numbers in small diameter tubes," *Heat Transf. Eng.*, vol. 24, no. 3, pp. 4–16, 2003.

[10] C. Y. Yap, C. K. Chua, Z. L. Dong, Z. H. Liu, D. Q. Zhang, L. E. Loh, and S. L. Sing, "Review of selective laser melting: Materials and applications," *Appl. Phys. Rev.*, vol. 2, no. 4, 2015.

[11] A. E. Patterson, S. L. Messimer, and P. A. Farrington, "Overhanging Features and the SLM/DMLS Residual Stresses Problem: Review and Future Research Need," *Technologies*, vol. 5, no. 2, p. 15, 2017.

[12] "4 enterprises (who are not SpaceX) Using 3D Printing to reach space - 3D Printing Industry." [Online]. Available: https://3dprintingindustry.com/news/4-enterprises-not-spacex-using-3d-printing-reach-space-96578/. [Accessed: 20-Apr-2018].

[13] L. Thijs, M. L. Montero Sistiaga, R. Wauthle, Q. Xie, J. P. Kruth, and J. Van Humbeeck, "Strong morphological and crystallographic texture and resulting yield strength anisotropy in selective laser melted tantalum," *Acta Mater.*, vol. 61, no. 12, pp. 4657–4668, 2013.

[14] V. K. Balla, S. Banerjee, S. Bose, and A. Bandyopadhyay, "Direct laser processing of a tantalum coating on titanium for bone replacement structures," *Acta Biomaterialia*, vol. 6, no. 6. pp. 2329–2334, 2010.

[15] F. E. Boas and D. Fleischmann, "CT artifacts: causes and reduction techniques," *Imaging Med.*, vol. 4, no. 2, pp. 229–240, 2012.

[16] F. Romei and A. N. Grubišić, "High Performance Resistojet Thruster: STAR Status Update," in *Space Propulsion Conference*, 2018.

[17] F. Romei, A. Grubišić, and D. Gibbon, "Performance Testing and Evaluation of a High Temperature Xenon Resistojet Prototype Manufactured by Selective Laser Melting," pp. 1–12, 2017.

[18] "Inspection of components manufactured by metal additive manufacturing | µ-VIS: Multidisciplinary, Multiscale, Microtomographic Volume Imaging | University of Southampton." [Online]. Available: https://www.southampton.ac.uk/muvis/case-studies/inspection-of-components-manufactured-by-metal-additive-manufacturing.page. [Accessed: 20-Apr-2018].

[19] M. Robinson, A. N. Grubišić, and F. Romei, "Endurance Testing of the STAR Additively Manufactured Resistojet," in *Space Propulsion Conference*, 2018.

[20] "The ISO 4287:1997 Written Standard." [Online]. Available: http://www.imagemet.com/WebHelp6/Content/RoughnessAnalysis/RoughnessISO4287.htm. [Accessed: 17-Apr-2018].

[21] "Surface Texture Parameters - SoftGauges." [Online]. Available: http://resource.npl.co.uk/softgauges/SP_Surf_Para.htm. [Accessed: 17-Apr-2018].

[22] "Optical Profilers - How Optical Profilers Work." [Online]. Available: https://www.zygo.com/?/met/profilers/opticalprofilersabout.htm. [Accessed: 17-Apr-2018].

[23] "Alicona – That's metrology: InfiniteFocus." [Online]. Available: http://www.alicona.com/products/infinitefocus/. [Accessed: 17-Apr-2018].

[24] "Sa (Arithmetical Mean Height) | Area Roughness Parameters | Introduction To Roughness | KEYENCE America." [Online]. Available: https://www.keyence.com/ss/products/microscope/roughness/surface/parameters.jsp. [Accessed: 19-Apr-2018].

[25] "Custom 450/225 kVp Hutch | µ-VIS: Multidisciplinary, Multiscale, Microtomographic Volume Imaging | University of Southampton." [Online]. Available: https://www.southampton.ac.uk/muvis/about/equipment/hutch.page. [Accessed: 17-Apr-2018].